行政院國家科學委員會專題研究計畫　成果報告

總計畫(I)

計畫類別：整合型計畫
計畫編號：NSC93-2215-E-002-024-
執行期間：93 年 08 月 01 日至 94 年 07 月 31 日
執行單位：國立臺灣大學電子工程學研究所

計畫主持人：林浩雄
共同主持人：楊英杰，毛明華
計畫參與人員：蔡宗霖、李騏&#20120；、萬政典、吳德清、蘇立杰、王關鑑、余治浩、錢皓哲、邱科智、楊崇淵

報告類型：精簡報告

處理方式：本計畫可公開查詢

中　華　民　國 94 年 10 月 31 日

行政院國家科學委員會專題研究計畫成果報告

前瞻性量子元件

計畫編號: NSC-93-2125-E-002-024

執行期限:93/08/01~94/07/31

共同主持人: 林浩雄、楊英杰、毛明華

參與人員： 蔡宗霖、李騏亘、萬政典、吳德清、蘇立杰、王關鑑、余治浩、錢皓哲、邱科智、楊崇淵

執行單位: 國立台灣大學電子研究所、光電研究所

中文摘要

本計畫包括以分子束磊晶法在砷化鎵基板上成長銻砷化鎵/砷化鎵第二型量子井、砷化銦鎵/砷化銦量子點結構雷射二極體的研究、以及量子點雷射動態調變特性等研究。在第二型量子井的部分我們利用共振腔長度調整雷射波長，並利用雷射增益的計算來模擬銻砷化鎵/砷化鎵第二型量子井能帶排列的關係。我們獲致的$GaAs_{0.64}Sb_{0.36}$/GaAs量子井主動層其GaAsSb之彎曲係數為 -1.31 eV，而價電帶差與能隙差比為1.02。在量子點雷射結構的部分，我們發展了一種新型的耦合量子點主動層結構。與非耦合量子點結構相比，此種結構的雷射特性並沒有劣化，但其波長可以延長。在量子點雷射動態特性研究的部分，我們創新提出量子點雷射之小訊號等效電路，並且可使用P-SPICE來模擬阻抗響應與光學響應，並且藉由與已知的雷射調變特性模擬來驗證此模型的有效性。此外，研究量子點雷射雙能態頻譜動態解析也是首度被實驗觀察到。激發態雷射動作早於基態雷射行為，此與理論的模擬是一致的。

關鍵詞: 分子束磊晶，含銻化合物半導體，銻砷化鎵量子井，砷化銦量子點，量子點雷射，彎曲係數、價電帶差比、調變頻寬、雷射等效電路、雙能態現象。

Abstract

The studies of this project include the molecular beam epitaxial (MBE) growth of GaAsSb type-II quantum well (QW) and InGaAs/InAs quantum dot (QD), and the modulation properties of QD laser diodes. In the first portion, GaAsSb/GaAs type-II QW lasers were fabricated. Because of the band-bending effect, the emission wavelength of the laser has a blue-shift as the cavity length is shortened. We utilized this effect to investigate the band line-up of the GaAsSb/GaAs QW. Through a simulation based on solving the Poisson and Schrödinger equations simultaneously for the band structure and optical gain of GaAsSb/GaAs QW, we found that the valence band offset ratio (Q_v) of the unstrained $GaAs_{0.64}Sb_{0.36}$/GaAs is 1.02, and the unstrained band-gap bowing parameter of GaAsSb is -1.31 eV. For QD lasers, we present a novel coupled-QD structure. The structure contains two closely coupled InAs QD layers and one InGaAs capping layer on top QD layer. Cross-sectional TEM images reveal that the coupled-QDs have larger size and lower density as compared with the controlled sample. The laser of coupled-QD structure demonstrates longer emission wavelength and slightly higher threshold current density than its counterpart, which indicates the coupled-QD structure is promising for long wavelength applications. In the portion of the dynamic properties study, the small-signal equivalent circuit model of quantum-dot lasers is proposed for the first time. We use P-SPICE to simulate their impedance and optical responses. The validity of this model is confirmed by the well-known laser modulation properties. Finally, spectrally resolved dynamics of two-state lasing in QD lasers is also experimentally demonstrated for the first time in this study. The onset of excited-state lasing prior to ground-state lasing is consistent with our theoretical prediction.

Keywords: molecular beam epitaxy, Sb-based compound semiconductor, GaAsSb quantum well, InAs quantum dot, quantum-dot laser, bowing parameter, valence-band-offset ratio, modulation bandwidth, laser equivalent circuit, two-state phenomenon.

Introduction

Recently, GaAs based long-wavelength lasers have attracted great attentions and are recognized as the key light sources for the optical communication in the near future. These lasers include diluted-nitrides based InGaAsN quantum well (QW) lasers [1], type-II GaAsSb/GaAs QW lasers [2-3], and InAs quantum dot (QD) lasers [4]. To design the GaAsSb/GaAs QW lasers, knowledge of the band parameters is very essential. However, the studies on the band lineup between GaAs and GaAsSb give inconsistent results so far. In terms of GaAsSb/GaAs valence-band-offset

ratio Q_v, the reported values range from less than 1 (type-I) to 2.1 [5-6]. Particularly, in some recent reports, even weak type-I lineup was proposed for this alloy system [7-8]. The scattered results in band line-up may be imputable to the complicated band-bending effect [9] resulting from the spatial separation of electrons and holes in the type-II QW or weak type-I QW. In this study, we grew high-quality GaAsSb/GaAs QW lasers and characterized their cavity-length dependent behaviors. By comparing the behaviors with a theoretical calculation considering the band-bending effect and band renormalization, the best fitted band parameters are obtained.

Semiconductor quantum dots (QD) have emerged recently as a promising gain material in the active region for long-wavelength semiconductor lasers. These nanostructures have three-dimensional confinement potentials for the capture of charge carriers. Due to discrete energy spectrum with delta-function-like density of states [10], self-assemble QD thin films have attracted much attention on the new physical phenomenon of electronic systems and their potential applications in optoelectronics, such as lasers [11-14], optical memory structures [15-16], and infrared photodetectors [17-18]. In the past, we have demonstrated QD lasers with 1295 nm emission wavelength [19] and recorded modulation bandwidth [20]. In this report, we firstly proposed a novel coupled QD for laser active medium. When the intermediate GaAs layer between two InAs quantum dot (QD) stacks is reduced to the range of several nanometers, the QDs of the second stack will be aligned in the vertical direction and results in a couple of important features [21-24] which is beneficial to laser applications. In this study, we study the effect on QD lasers. Then, we will demonstrate the results of measurements of transient dynamics of two-state lasing. We also propose a small-signal equivalent circuit of QD lasers to simulate their modulation behavior[10].

Results and Discussions

In the study of GaAsSb/GaAs QW lasers, we used VG V80H solid source molecular beam epitaxy (SSMBE) to grow the structures. As_4 and Sb_1 sources were from a Riber VAC500 valve cracker and an EPI 175 Sb cracker, respectively. The growth temperature of GaAsSb/ GaAs QW was 500°C, and the growth rate was ~ 1 μm/hr. The active medium of the laser is a 7-nm-thick GaAsSb QW with 80-nm-thick GaAs barrier. $Al_{0.6}Ga_{0.4}As$ served as the cladding layers and they were grown at 580°C. The active layer was enclosed within an undoped separate confinement hetero- structure (SCH) composed of two 100-nm-thick AlGaAs graded index (GRIN) layers. By increasing Sb content in the GaAsSb well, the PL emission wavelength can be extended to 1300 nm. 50-μm-wide broad stripe lasers with different cavity lengths were fabricated. The fabricated GaAsSb/GaAs QW lasers showed very low threshold currents. The dependence of inverse external quantum efficiency versus cavity length is depicted in Fig. 1. As can be seen, the internal quantum efficiency is 31% and the internal loss is 4.8 cm^{-1} for the QW lasers. The obtained internal losses were then used to calculate the modal gain of each laser. In the calculation, the reflectivity of the as-cleaved mirror was set to be 0.32.

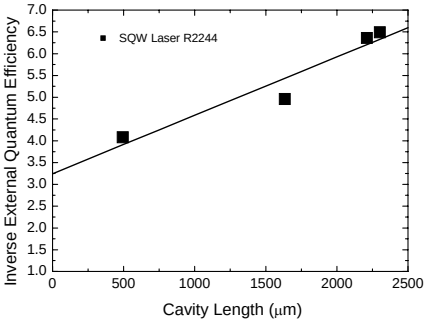

Fig.1 Inverse external quantum efficiency as a function of cavity length plots.

To begin with the optical gain calculation, we chose the values for the band-gap energy of GaAsSb and the valence-band-offset ratio of GaAsSb/GaAs QW to construct the flat-band structure of the active region. Then, we solved the Schrödinger equation and Poisson equation simultaneously for the strained GaAsSb/ GaAs QWs with a given carrier density. In our calculation, only one kind of electrons and holes with isotropic, parabolic dispersion is assumed to exist, thus neglecting most of the band-structure complications of the valence subbands. And we consider the band renormalization effect by including the relative terms into the potential energy term of the Schrödinger equation:

$$U_r = V_r + V_{H,r} + V_{XC,r} \quad (1)$$

where V_r is the GaAsSb/GaAs QW potential energy, and $V_{H,r}$, $V_{XC,r}$ are space charge induced Hartree term and many body effect induced exchange-correlation term respectively. The suffix r indicates a position along the growth direction. To calculate the exchange-correlation term $V_{XC,r}$, we use the following formula [25],

$$V_{xc,r} = \frac{-2}{\pi\alpha r_0}[1 + 0.0545 r_0 \ln(1 + 11.4 r_0)] \quad (2)$$

where parameter α is defined by $\alpha = (4/9\pi)^{1/3}$, and r_0 is the dimensionless electron sphere radius defined by $r_0 = r/a_0^*$, a_0^* is the effective Bohr radius, and r is defined as $(3/4n\pi)^{1/3}$ for bulk 3D carriers or $(n\pi)^{1/2}$ for quantum well 2D carriers. However, because the thickness of quantum well is finite, the carriers in the quantum well are not strictly 2D systems. Thus, as the well width increases, three-dimensional characteristics

will gradually emerge and become dominant. In the GaAsSb/GaAs quantum well of the laser for analysis, electrons are confined in the 80-nm-thick GaAs layer and holes are confined in the 7-nm-thick GaAsSb layer. Therefore, we treat electrons as 3D carriers and holes as 2D carriers for their own effective confines. In this self-consistent calculation, 16 electron sub-bands and 4 heavy hole sub-bands were considered. The calculation gives not only the space charge field profile but also the wavefunction and carrier density for each subband. The material gain per unit length for electron sub-band 2 and hole sub-band 1, g_{21}, can thus be calculated using the following formula [26],

$$g_{21} = \frac{\pi q^2 \hbar}{nc\varepsilon_0 m_0^2 E_{21}} |M_T|^2 \rho_r (E_{21})(f_2 - f_1) \qquad (3)$$

where M_T is the transition matrix element, ρ_r is the reduced density of state, f_1 and f_2 are the occupation probabilities of subband 1 and 2. Other notations can be referred to [26]. The total gain at transition energy E_{21} can be found by summing over all possible subband pairs. Scan the transition energy from the lowest subband pairs to 1.4 eV, one can find the gain spectrum. Fig. 2 shows the calculated modal gain spectrums for GaAsSb/GaAs single QW laser under carrier injection levels ranging from 2.5 to 5.3 × 10^{12}/cm^2. The confinement factor of the laser is 0.0215. As can be seen, when carrier density increases, gain peak shifts toward short wavelength significantly. It is due to the band-bending effect taking place in the interface of GaAsSb/GaAs quantum well. From Fig. 2, one can easily find the relation between the peak modal gain and peak wavelength. When a laser reaches oscillation, its modal gain is just equal to the total loss, which is the sum of the mirror loss and the internal loss. For a GaAsSb/ GaAs single QW laser with a cavity length of L, the mirror loss is (1/L)ln(1/R), while the internal loss obtained from Fig. 1 is 4.8 cm^{-1}. Therefore, the modal gain for GaAsSb/GaAs lasers is (1.139/L + 4.8) cm^{-1}. Through this formula, we can obtain the relation between the lasing wavelength and the cavity length. The results are shown in Fig. 3. For comparison, the experimental data is also depicted in the figure. Basically, the curvature of the curve is independent of GaAsSb band-gap energy. Changing the band-gap energy only gives the curve a vertical shift. However, changing the valence band offset ratio of the GaAsSb/GaAs QW, Q_v, not only provides the curve a vertical shift, but also significantly affects the curvature of the curve as can be seen in Fig. 3. We repeatedly adjusted the bow parameter and valence-band-offset ratio until the difference between the experimental and theoretical results was minimized. Three curves with different Q_v are depicted in Fig. 3. As can be seen, the calculated curve with Q_v = 1.02 is in good agreement with the experimental data. The input parameters for this best-fitted calculation are listed as follows. The unstrained band-gap energy for GaAsSb in single QW

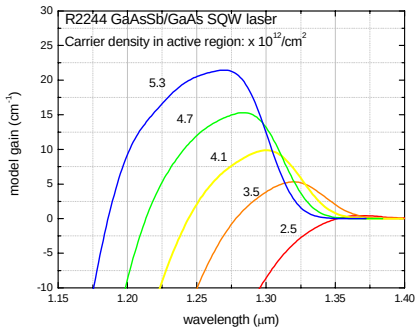

Fig. 2 Calculated modal gain spectrums for GaAsSb/ GaAs SQW laser. The gain peak clearly shows a blue shift as the carrier density increases.

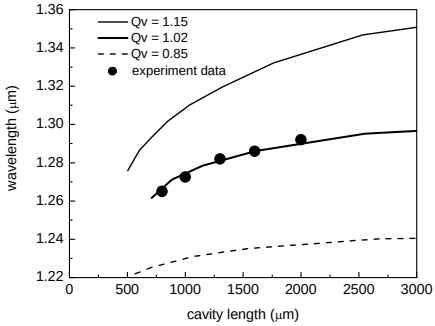

Fig.3 Lasing wavelength as a function of cavity length of GaAsSb/GaAs laser. Curve represents the simulation results while the circles represent the experimental data.

is 0.869 eV. Note that the Sb compositions for this sample measured by XRD are 0.36. Combine with the well-known band-gap energy of GaAs and GaSb, we obtain a bowing parameter of -1.31 eV. Again, the best-fitted valence-band-offset ratio of GaAsSb/GaAs QW is 1.02.

The QD lasers were grown on n$^+$ (100) GaAs substrates by VG V80H SSMBE system. For comparison, two laser samples, R2264 (with coupled QD layers) and R2265 (with normal QD layers) were grown. Both lasers are separated-confinement lasers and their active mediums are composed of two QD stacks separated by a GaAs spacer layer. The QD growth was started at 485^{o}C. For coupled QD sample, 2 monolayers (ML) seed InAs QD layer was deposited and followed by the growth of a 6-nm-thick GaAs spacer layer. Next, the substrate temperature was raised to 590^{o}C for 5 minutes to anneal the QDs. The temperature was then cooled down to 485^{o}C for the deposition of the second InAs layer, followed by the overgrowth of the 6-ML-thick $In_{0.33}Ga_{0.67}As$ capping layer. The capping layer was deposited by GaAs/InAs sequential binary growth method, which was in the sequence of the following steps: 0.5 ML Ga deposition, 5 sec As_2 illumination and 0.25 ML InAs deposition. Between the steps, there was a 2.5 sec interruption without As_2 protection. This cycle was repeated until the designed thickness of the InGaAs layer was reached. The growth rate for QDs was

0.085ML/s [19]. Normal QD layer has similar growth procedures except the steps for the 6-nm-thick GaAs spacer layer and the second InAs QD layer. The InGaAs capping layer was directly overgrown on the seed InAs QD layer, and their deposition conditions were all the same as those for the corresponded steps used for the coupled-QD sample. Detailed laser structures of R2264 and R2265 are summarized in Fig. 4(a) and (b), respectively. After the growth, standard photolithography, chemical etching and metallization processes were used to fabricate 50-μm-wide as cleaved broad area lasers.

R2264 QD lasers (2 QD layer)

100 nm GaAs (Be 2e19 cm^{-3})
$Al_{0.4}Ga_{0.4}As \rightarrow Al_{0.08}Ga_{0.92}As$ (Be 2e18cm^{-3}) 20nm
1.1 um $Al_{0.4}Ga_{0.4}As$ (Be 2e18 cm^{-3})
0.4 um $Al_{0.4}Ga_{0.4}As$ (Be 1e17 cm^{-3})
115nm GaAs (undoped)
2ML InAs / 60Å GaAs / 2ML InAs / 6ML $In_{0.33}Ga_{0.67}As$
34 nm GaAs
2ML InAs / 60Å GaAs / 2ML InAs / 6ML $In_{0.33}Ga_{0.67}As$
115 nm GaAs (undoped)
0.4 um $Al_{0.4}Ga_{0.4}As$ (Si 2e17 cm^{-3})
1.1 um $Al_{0.4}Ga_{0.4}As$ (Si 2e18 cm^{-3})
$Al_{0.08}Ga_{0.92}As \rightarrow Al_{0.4}Ga_{0.4}As$ (Si 2e18cm^{-3})
500 nm GaAs (Si 2e18cm^{-3})
N+ GaAs Substrate

R2265 QD lasers (2 QD layer)

100 nm GaAs (Be 2e19 cm^{-3})
$Al_{0.4}Ga_{0.4}As \rightarrow Al_{0.08}Ga_{0.92}As$ (Be 2e18cm^{-3}) 20nm
1.1 um $Al_{0.4}Ga_{0.4}As$ (Be 2e18 cm^{-3})
0.4 um $Al_{0.4}Ga_{0.4}As$ (Be 1e17 cm^{-3})
115nm GaAs (undoped)
2ML InAs / 6ML $In_{0.33}Ga_{0.67}As$
62nm GaAs
2ML InAs / 6ML $In_{0.33}Ga_{0.67}As$
115 nm GaAs (undoped)
0.4 um $Al_{0.4}Ga_{0.4}As$ (Si 2e17 cm^{-3})
1.1 um $Al_{0.4}Ga_{0.4}As$ (Si 2e18 cm^{-3})
$Al_{0.08}Ga_{0.92}As \rightarrow Al_{0.4}Ga_{0.4}As$ (Si 2e18cm^{-3}) 20 nm
500 nm GaAs (Si 2e18cm^{-3})
N+ GaAs Substrate

Fig. 4. Layer structures of (a) coupled-QD laser R2264 and (b) normal-QD laser R2265.

The cross-sectional TEM images of the active regions are shown in Fig. 5(a) and (b). As can be seen in Fig. 5(a), for each coupled QD stack, the positions of the upper InAs QD with its InGaAs capping layer and the bottom seed InAs QD are in good alignment. Furthermore, as comparing the sizes of the coupled QDs and normal QDs, it is clearly that the coupled QDs have larger size both in lateral and vertical direction. These findings imply that when the upper QD of the coupled QD structure was being deposited, the In atoms preferentially accumulated on the sites where the bottom seed QDs were buried. Because the

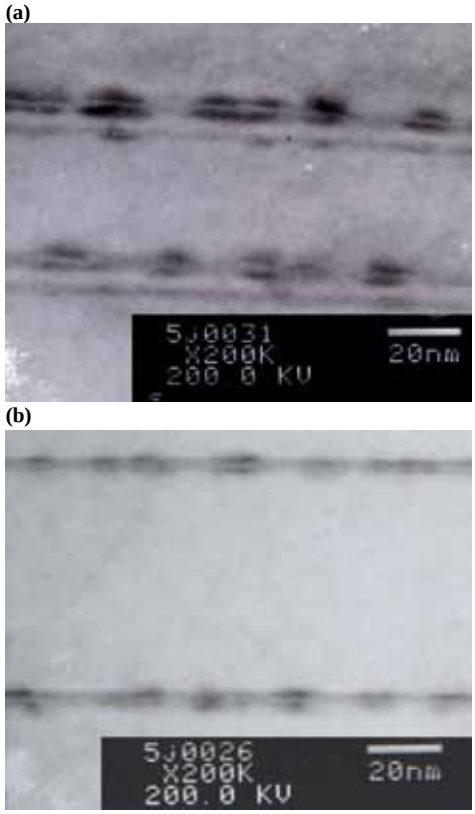

Fig. 5 Cross-sectional TEM image of (a) R2264 (b) R2265.

buried QDs make the upper GaAs tensile strained, the InAs island formed on this region would have lower lattice mismatch to its bottom layer. As a result, larger InAs QDs are formed preferentially on the larger-strain-field region; the formation on the small-strain-field region is prevented [22]. The figures also reveal that the coupled-QD sample has lower dot density than the normal-QD sample. From FESEM image taken from another sample which has only coupled-QDs grown on the top by the same growth procedure, the dot density for coupled-QD layer is ~ $3.4 \times 10^{10}/cm^2$, while the density of the normal-QD sample estimated from the same method is ~$5.1 \times 10^{10}/cm^2$.

Fig. 6 (a) and (b) show the pulsed L-I curve of 2-mm-long coupled-QD laser R2264 and normal-QD laser R2265, respectively. The pulse width and repetition rate are 4μs and 500 Hz. As can be seen, the threshold current density and external quantum efficiency are $133A/cm^2$ and 31.2% for R2264, $127 A/cm^2$ and 47.5% for R2265, in respectively. Basically, the coupled-QD device demonstrates slightly higher threshold current density and lower quantum efficiency than the normal-QD device, which means that the modal gains of both devices are almost the same. Further analysis on the model gain also indicates that the transparency current densities per QD layer of R2264 and R2265 are 8.3 and 9.6 A/cm^2. Both values are very close to the theoretical calculation, which implies the very good material quality of the lasers. If we assume that the QDs in

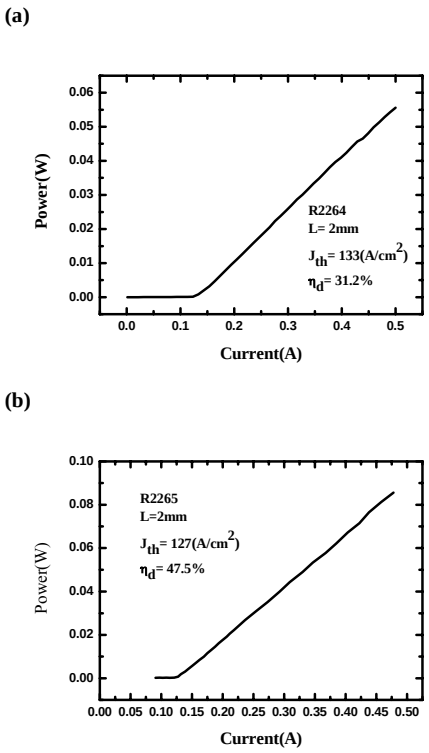

Fig. 6 L-I curve of (a) coupled-QD laser R2264 (b) normal-QD laser R2265.

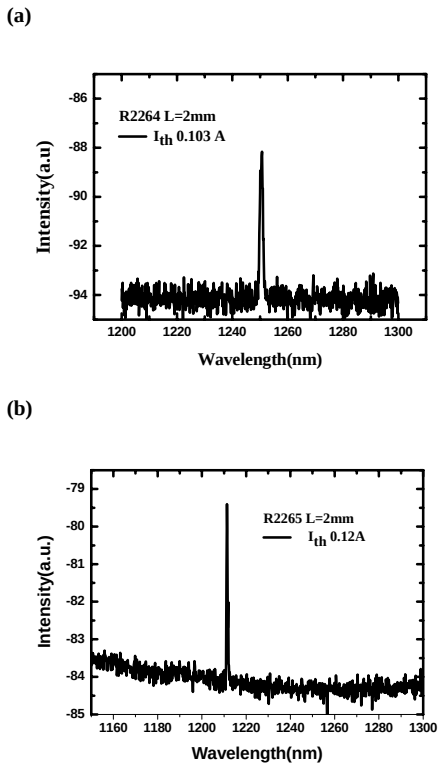

Fig. 7 EL spectrum of (a) coupled-QD laser R2264 (b) normal-QD laser R2265.

both devices sustained the same In/Ga intermixing and desorption after the capping of InGaAs layer and the carriers in the coupled QDs are mainly confined in the upper QDs, then the total volumes of the capped QDs in both devices should be equal. It means that both lasers have the same optical confinement factor and therefore their material gains are very close to each other. Notice that in QD lasers, besides the dot density, the inhomogeneity and the transition matrix element of the QDs also affect the material gain. Though the dot density in the coupled-QD device is only two-third of that of the normal-QD device, the laser still possesses comparable laser performances. It implies that the coupled QDs may have better size homogeneity or higher transition matrix element. Low temperature PL spectrums of both devices were measured. The coupled QDs do not have narrower FWHM. Therefore, we conclude that the coupled QDs may have higher transition matrix element than the normal QDs. Room temperature electroluminescence (EL) spectrums for R2264 and R2265 are shown in Fig. 7 (a) and (b). The emission wavelength for R2264 and R2265 are at 1250 and 1211 nm respectively. The longer emission wavelength of the coupled-QD laser is attributed to its large QD size which has been observed from Fig. 5. In addition, the intermediate GaAs layer between the two InAs QD stacks is only 6 nm, electron coupling between the seed and the capped QDs may further reduce the transition energy [27].

Rate-equation modeling has been widely used in theoretical simulation of dynamic properties of laser diodes. It is a highly flexible tool capable of dealing with complex physical systems, including QD lasers. On the other hand, SPICE represents a powerful and reliable simulator for circuit analysis, such as laser-driver circuit and package effects. It would be advantageous to combine these tools to provide a unified detailed description for the whole transmitter module. Although there were equivalent circuit models for bulk and quantum-well lasers proposed in the literature [28-30], there are no such circuit models for QD lasers up to now. Starting from rate equations, this work presents for the first time the small-signal equivalent circuit model of quantum-dot lasers with inclusion of their important physical properties, such as the inhomogeneous broadening. This circuit model, simulating the impedance and optical responses of QD lasers, will be easily incorporated into another circuit of higher degree of integration for SPICE analysis and design of transmitter modules in the future. To build up this model, QDs are divided into *n* groups while only some of them (from *i*-th to *j*-th group) contribute to lasing. From Fig. 8(a), (b), we observe the resonant frequency increased, while the impedance decreased with increasing bias current.

The simulation result is fully consistent with the common frequency-domain characteristics of laser diodes. This model is then further applied to simulate two QD lasers with different inhomogeneous broadening linewidth, namely FWHM of 15 meV and 30 meV, respectively. From Fig. 8 (c), we see clearly that the QD laser with 15 meV FWHM of

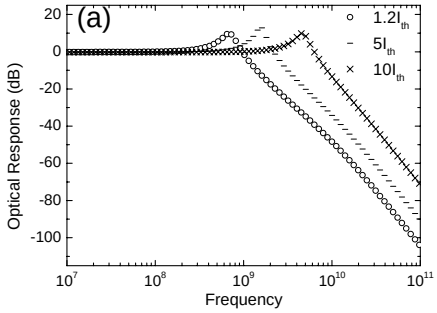

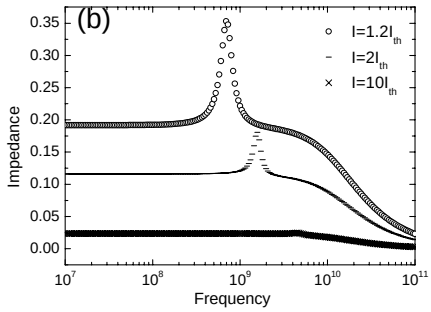

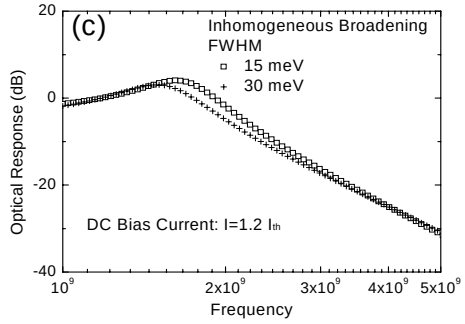

Fig. 8 Simulated frequency responses of QD lasers (a) optical response, (b) impedance response, (c) optical modulation response of two QD lasers with different inhomogeneus broadening linewidth.

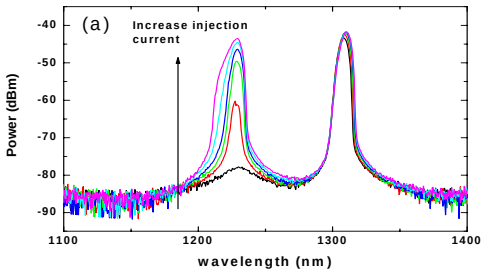

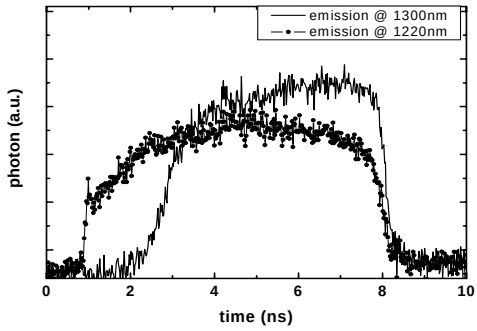

Fig. 9 (a) EL spectra under various current densities (b) measured photon transient of GS and ES.

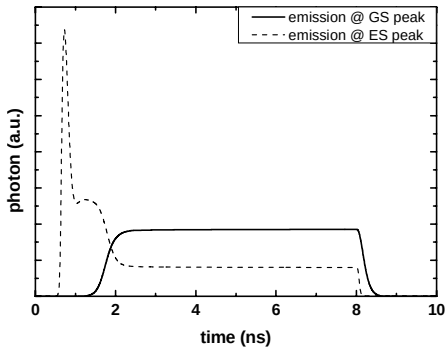

Fig. 10 Simulated photon transients using a rate-equation threshold current density.

inhomogeneous broadening linewidth due to its more uniform size distribution shows a higher resonant frequency and larger modulation bandwidth. This is consistent with the prediction of rate-equation modeling [31].

Recently, experimental observation of simultaneous lasing in steady state from ground states and excited states in QD lasers has been reported [32-34]. This effect was studied also theoretically, both in steady state and in transient behavior [35]. However, these is no experimental investigation about the individual transient responses of GS and ES, respectively, from two-state-lasing QD lasers up to now. Fig. 9(a) shows the EL spectrum under different injection current densities. GS lasing is observed at 1.3 μm, while ES lasing is around 1.22 μm. Fig. 9(b) shows individual large-signal modulation measurement results of GS and ES respectively. The onset of ES lasing prior to GS lasing is experimentally observed for the first time. This interesting feature can be further analyzed with the help of numerical simulation. Fig. 10 shows our theoretical prediction of two-state-lasing dynamics in QD lasers [31]. Excited state can achieve lasing earlier than GS lasing although their emission intensity is lower in the steady state. This phenomenon is consistent with the measurement results in Fig. 9. Under certain conditions, especially when the optical loss level is close to GS saturation gain, ES emission will play a more important role in QD laser transient response than in static measurement.

Conclusions

We have grown GaAsSb/GaAs type-II lasers and analyzed the band lineup of the QW. Due to the space charge electric field in the QW, the lasing wavelength

showed a blue shift as the cavity length decreased. This phenomenon was simulated and utilized to derive the band structure of the QW. The best-fitted bowing parameter of GaAsSb alloy and valence-band-offset ratio of GaAsSb/GaAs QW are -1.31 eV and 1.02 in respectively. The growth and characteristics of a novel coupled-QD laser are reported. In comparison with the normal QDs, the coupled QDs have larger size but lower dot density. However, the lower dot density does not significantly degrade the laser performance. The most important is the larger size make the coupled-QD laser has longer emission wavelength, which is 1250 nm. The wavelength of the controlled normal-QD device is 1211 nm. The small-signal equivalent circuit model of QD lasers with multi-mode lasing is proposed for the first time in this work. P-SPICE is applied to simulate their impedance and optical responses. This model is confirmed by the well-known laser modulation properties and its ability to show some unique features, such as inhomogeneous broadening, of quantum-dot lasers has been verified successfully. Furthermore, spectrally-resolved dynamics of two-state lasing in QD laser is experimentally demonstrated for the first time in this study. The onset of ES lasing prior to GS lasing is consistent with our theoretical simulation.

References

[1] T. Takeuchi, Y.-L. Chang, M. H. Leary, D. E. Mars, A. Tandon, C.-K. Lin, R. Twist, S. Belov, D. P. Bour, M. R. T. Tan, Y.-K. Song, L. Mantese and H.-C. Luan,, Proceedings of 16th LEOS annual meeting, 35 (2003).

[2] K. Nishi, T. Anan, M. Yamada, K. Kurihara, K. Tokutome, A. Kamei, and S. Sugou, 2001 Digest of the LEOS Summer Tropical Meetings, 15. (2001)

[3] P. W. Liu, M. H. Lee, H. H. Lin, and J. R. Chen, Electron. Lett. **38**, 1354 (2002).

[4] N. Ledentsov, Proceedings of 2002 IEDMS, 2 (2002).

[5] M. Peter, K. Winkler, M. Maier, H. Herres, J. Wagner, D. Fekete, K. H. Bachem, and D. Richards, *Appl. Phys. Lett.*, **67**, 2639, (1995).

[6] R. Teissier, D. Sicault, J. C. Harmand, G. Ungaro, G. Le Roux, and L. Largeau, *J. Appl. Phys.*, **89**, 5473, (2001).

[7] J. B. Wang, S. R. Johnson, S. A. Chaparro, D. Ding, Y. Gao, Yu. G. Sadofyev, and Y.-H. Zhang, *Phys. Rev. B.* **70**, 195339. (2004)

[8] R. T. Senger, K. K. Bajaj, E. D. Jones, N. A. Modine, K. E. Waldrp, F. Jalali, J. F. Klem, G. M. Peake, X. Wei, and S. W. Tozer, *Appl.* Phys. Lett. , pp. 2614-2616. (2003)

[9] D. Vignaud, X. Wallart, F. Mollot, and B. Sermage, J. Appl. Phys. 84, 2138, (1998).

[10] Y. Arakawa and H. Sakaki, *Appl. Phys. Lett.* **40**, 939 (1982).

[11] D. Bimberg, M. Grundmann, and N. N. Ledentsov, Quantum Dot Heterostructures, Wiley (1999).

[12] A. E. Zhukov, A. R. Kovsh, V. M. Ustinov, Y. M. Shernyakov, S. S. Mikhrin, N. A. Maleev, E. Y. Kondrat'eva, D. A. Livshits, M. V. Maximov, B. V. Volovik, .D. A. Bedarev, Y. G. Musikhin, N. N. Ledentsov, P. S. Kop'ev, Z. I. Alferov, and D. Bimberg. *IEEE Phot. Tech. Lett.* **11**, 1345 (1999).

[13] N. N. Ledentsov, M. Grundmann, F. Heinrichsdorff, D. Bimberg, V. M. Ustinov, A. E. Zhukov, M. V. Maximov, Z. I. Alferov, and J. A. Lott, *IEEE J. Sel. Top. Quantum Electron.* **6**, 439 (2000).

[14] D. L. Huffaker, G. Park, Z. Zou, O. B. Shchekin, and D. G. Deppe, *Appl. Phys. Lett.* **73**, 2564 (1998).

[15] J. J. Finley, M. Skalitz, M. Arzberger, A. Zrenner, G. Böhm, and G. Abstreiter, *Appl. Phys. Lett.* **73**, 2618 (1998).

[16] T. Lundstrom, W. Schoenfeld, H. Lee, and P. M. Petroff, *Science* **286**, 2312 (1999).

[17] L. Chu, A. Zrenner, G. Böhm, and G. Abstreiter, *Appl. Phys. Lett.* **75**, 3599 (1999).

[18] L. Chu, A. Zrenner, G. Böhm, and G. Abstreiter, *Appl. Phys. Lett.* **76**, 1944 (2000).

[19] F. Y. Chang, C.C. Wu, and H. H. Lin, *Appl. Phys. Lett*. 82, 4477 (2003).

[20] M.-H. Mao, T.-Y. Wu, F.-Y. Chang, and H.-H. Lin, 2003 IEEE LEOS Annual Meeting, Tucson, Oct. 2003.

[21] M. Sugawara, *Self-Assembled InGaAs/GaAs Quantum Dots* (Acaemic Press, 1999).

[22] O. G. Schmidt, N. Kirstaedter, N. N. Ledentsov, M. H. Mao, D.Bimberg, V. M. Ustinov, A. Y. Egorov, A. E. Zhukov, M. V. Maximov, P. S. Kopev, and Z. I. Alferov, *Electron. Letter*. 32, 1302 (1996).

[23] G. S. Solomon, J.A. Trezza, A.F. Marshall, and J.S. Harris, *Phys. Rev. Letter*. 76, 952 (1996).

[24] I. Mukhametzhanov, Z. Wei, R. Heitz, A. Madhukar, *Appl. Phys. Lett.* 75, 85 (1999).

[25] O.Gunnarsson and B.I. Lundqvist, *Phys. Rev. B.* **13**, 10, 1976.

[26] L. A. Coldren and S. W. Corzine, *Diode lasers and photonic integrated circuits*, (John Wiley and Sons, 1995).

[27] M. O. Lipinski, H. Schuler, O.G. Schmidt, and K. Eberl and N. Y. Jin-Phillipp 77, 1789 (2000).

[28] C. Harder, J. Katz, J. Shacham, and A. Yariv, "Noise Equivalent Circuit of Semiconductor Laser Diode," *IEEE J. Quantum Electron.* **QE-18,** 333 (1982).

[29] R. S. Tucker and D. J. Pope, *IEEE J. Quantum Electron.* **QE-19**, 1179 (1983).

[30] O. Kibar, D. V. Blerkom, C. Fan, P. J. Marchand, and S. C. Esener, *Appl. Opt.* **37,** 613 (1998).

[31] H.-T. Chen, W.-H. Hsieh, M.-H. Mao, *CLEO/Pacific Rim*, Taipei, Taiwan (2003).

[32] M.-H. Mao, L.-C. Su, K.-C. Wang, W.-S. Liu, P.-C. Chiu, J.-I. Chyi, IEEE LEOS Annual Meeting, Sydney, 2005.

[33] M. Sugawara, N. Hatori, E. Ebe, M. Ishida, Y. Arakawa, T. Akiyama, K. Otsubo and Y. Nakata, *J. Appl. Phys.* **97**, 043523 (2005)

[34] M. V. Maximov, L. V. Asryan, Yu. M. Shernyakov, A. F. Tsatsul'nikov, I. N. Kaiander, V. V. Nikolaev, A. R. Kovsh, S. S. Mikhrin, V. M. Ustinov, A. E. Zhukov, Zh. I. Alferov, N. N. Ledenstov and D. Bimberg, *IEEE J. Quantum. Electron.* **37**, 676 (2001)

[35] A. Markus, J. X. Chen, C. Paranthoen and A. Fiore, *Appl. Phys. Lett.* **82**, 1818 (2003)